New Results on Bare-Tether Current

ROBERT D. ESTES

Harvard-Smithsonian Center for Astrophysics, Cambridge, Massachusetts

JUAN R. SANMARTIN

ETSI Aeronáuticos, Universidad Politécnica de Madrid, Madrid, Spain

Recent results on the validity of the orbital-motion-limited (OML) regime of cylindrical Langmuir probes, which are essential for bare-tether applications, are extended to show how the current lags behind the OML value beyond the OML regime, and the possible effects of motion of the probe relative to the plasma.

The electron current I to a long cylinder at rest in a collisionless, unmagnetized, Maxwellian plasma of density N_∞ and temperatures T_e and T_i, may be written as

$I = I_{th} \times$ *a function of* R/λ_{De}, $e\Phi_P/kT_e$, T_i/T_e.

Here, $I_{th} \equiv 2\pi RLeN_\infty\sqrt{kT_e/2\pi m_e}$ is the random or thermal current, $\lambda_{De} \equiv \sqrt{kT_e/4\pi e^2 N_\infty}$ is the Debye length, and R, L, and Φ_P are probe radius, length, and bias, respectively. For cylinders thin enough, however, I/I_{th} only depends on $e\Phi_P/kT_e$. This is the orbital-motion-limited (OML) regime; at high bias one has

$$I_{OML} \approx I_{th} \times \sqrt{4e\Phi_P/\pi kT_e} = 2RLeN_\infty\sqrt{2e\Phi_P/m_e}\ , \quad (e\Phi_p >> kT_e)\ . \tag{1}$$

There is a maximum radius, R_{max}, for the OML regime to hold with other parameters fixed,[1,2] the ratio I/I_{OML} dropping below unity when R goes beyond R_{max}. The way that ratio drops below unity is of interest for the design of bare (uninsulated) tethers.[3,4]

In general, determining electron trajectories to obtain I requires solving Poisson's equation for $\Phi(r)$,

$$\frac{\lambda_{De}^2}{r}\frac{d}{dr}r\frac{d}{dr}\left(\frac{e\Phi}{kT_e}\right) = \frac{N_e}{N_\infty} - \frac{N_i}{N_\infty} \approx \frac{N_e}{N_\infty} - \exp\left(-\frac{e\Phi}{kT_i}\right), \tag{2}$$

with boundary conditions $\Phi = \Phi_p > 0$ at $r = R$, $\Phi \to 0$ as $r \to \infty$. The Boltzmann law used for the repelled-particle density N_i is quite accurate for the $e\Phi_p >> kT_i, kT_e$ values of interest here. The basic problem in probe theory lies in the attracted-particle density N_e.

Since the Vlasov equation conserves the electron distribution function $f(\mathbf{r},\mathbf{v})$ along orbits, and electrons trapped in bounded orbits may be ignored,[2] we have $f(\mathbf{r},\mathbf{v}) = f_M(v_\infty)$ (undisturbed Maxwellian) if the $\mathbf{r},\mathbf{v}$ orbit, traced back in time, reaches infinity, and $f(\mathbf{r},\mathbf{v}) = 0$ otherwise. Since both axial velocity v_z, and transverse energy (Fig.1)

$$\frac{m_e}{2}v_r^2 + \frac{m_e}{2}v_\theta^{\,2} - e\Phi \equiv E = \frac{m_e}{2}v_\infty^{\,2} - \frac{m_e}{2}v_z^{\,2}, \tag{3}$$

are also conserved along orbits, values $\mathbf{r},\mathbf{v}$ determine v_∞ and f_M in terms of the local potential $\Phi(r)$; the density N_e at a radius r is then obtained by integrating f_M over appropriate velocity ranges.[5] A change of variables v_r, $v_\theta \to E$, $J \equiv m_e r v_\theta$, and a trivial v_z-integration yield

$$N_e = N_\infty \iint \frac{\exp(-E/kT_e)dEdJ}{\pi kT_e\sqrt{J_r^2(E) - J^2}}\ , \tag{4}$$

where the J-integral covers just positive values, and we define

$$J_r^2(E) \equiv 2m_e r^2[E + e\Phi(r)]\ . \tag{5}$$

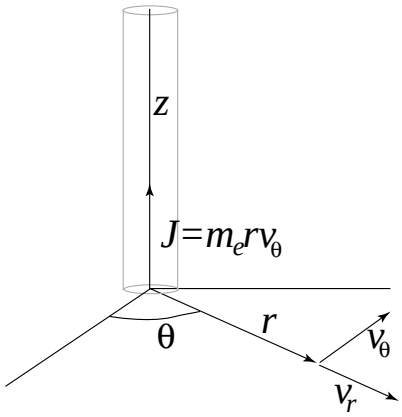

Figure 1. Geometry of cylindrical probe and electron motion.

The E-integral also covers positive values and is carried out once for $v_r < 0$ (incoming electrons) and again for $v_r > 0$ (electrons that turn outwards at a radius between r and R).

An incoming electron of energy E will only reach r if $v_{r'}^2$ is positive throughout the entire range $r < r' < \infty$; since J is also conserved, its range of integration will be

$$0 < J < J_r^*(E) \equiv \textit{minimum}\ \{\ J_{r'}(E)\ ;\ r \le r' < \infty\ \}. \tag{6}$$

If the minimum occurs at some $r' > r$, electrons in the range $J_r^*(E) < J < J_r(E)$, for which v_r^2 would actually be positive at r, never reach r and are thus excluded from the J-integral (there is an effective potential barrier at r, for energy E). The J-range of integration for an E-electron outgoing at r is $J_R^*(E) < J < J_r^*(E)$, because electrons in the range $0 < J < J_R^*(E)$ disappear at the probe. Equation (4) may now be written as

$$\frac{N_e}{N_\infty} = \int_0^\infty \frac{dE}{\pi kT_e}\exp\left(\frac{-E}{kT_e}\right)\left[2\sin^{-1}\frac{J_r^*(E)}{J_r(E)} - \sin^{-1}\frac{J_R^*(E)}{J_r(E)}\right]. \tag{7}$$

The current itself is easily found to be

$$I = 2RLeN_\infty \sqrt{\frac{2e\Phi_P}{m_e}} \times \int_0^\infty \frac{dE}{kT_e} \exp\left(\frac{-E}{kT_e}\right) \frac{J_R{}^*(E)}{J_R(0)}. \qquad (8)$$

A hypothetical potential with no barriers at all [$J_r^*(E) = J_r(E)$ for $0 \le E < \infty$, $R \le r < \infty$] would everywhere reduce N_e in (7) to a function of the local radius and potential. As we shall now see, however, actual potentials behave differently. Note that in order to have $J_r^*(E) = J_r(E)$ in the entire range $0 \le E < \infty$ at a particular r, it suffices to have $J_r^*(0) = J_r(0)$. Using $J_r^2(0) \propto r^2\Phi(r)$, it follows from (6) that the condition of no barrier at a radius r is

$$r^2\Phi(r) \le r'^2\Phi(r') \; (r \le r' < \infty). \qquad (9)$$

There are two consequences of that simple result: First, the condition of maximum current in (8), $J_R^*(E) = J_R(E)$ for $0 \le E < \infty$ (no potential barriers just at R) is satisfied if

$$R^2\Phi_p \le r^2\Phi(r). \quad (R \le r < \infty). \qquad (10)$$

This is the OML current; with $E \sim kT_e << e\Phi_p$, we have $J_R(E) \approx J_R(0)$ in Eq. (8), recovering (1). Secondly, a potential satisfying the condition

$$d(r^2\Phi)/dr \ge 0 \; , \; r_0 \le r < \infty, \qquad (11)$$

for some radius r_0, has potential barrier at no radius beyond r_0,

$$J_r^*(E) = J_r(E) \text{ for } 0 \le E < \infty, \; r_0 \le r < \infty. \qquad (12)$$

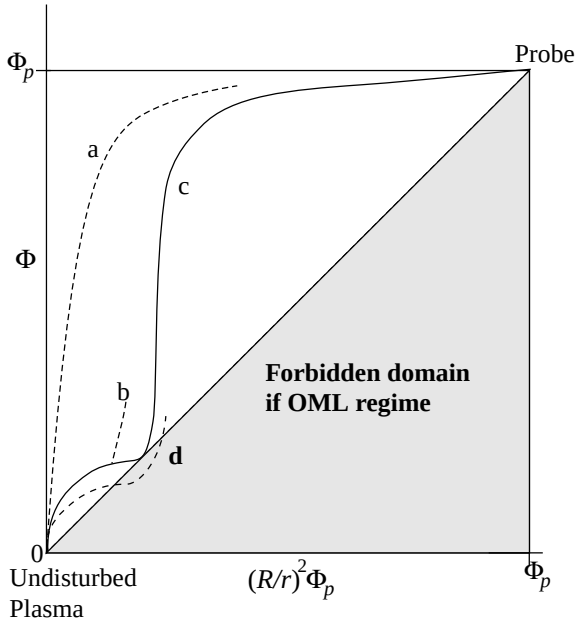

Figure 2. Schematics of potential Φ versus $\Phi_p(R/r)^2$ for profiles a and b ($R < R_{max}$), c ($R = R_{max}$), and d ($R > R_{max}$), with R_{max} the largest radius for the OML regime to hold. The hypothetical profile a would have no potential barriers.

Both consequences are conveniently illustrated by displaying Φ versus $\Phi_p R^2/r^2$ for potential profiles (Fig.2). Clearly, profiles *a*-c would lie in the OML regime, whereas *d* would not. Also, cases *b*-*d*, which are schematics of actual profiles, present property (11), r_0 being the radius where the ordinate-to-abscissa ratio in the figure, $\Phi/(\Phi_P R^2/r^2)$, goes through a minimum, then increasing monotonically when moving to the left past the minimum. Profile *c*, just touching the diagonal in the figure, corresponds to the case of maximum radius, R_{max}.[1,2] The extreme condition $J_r^*(E) = J_r(E)$ for $0 \le E < \infty$, $R \le r < \infty$, requiring a positive $d(r^2\Phi)/dr$ throughout, is, of course, more restrictive, and is only satisfied by the hypothetical profile *a*.

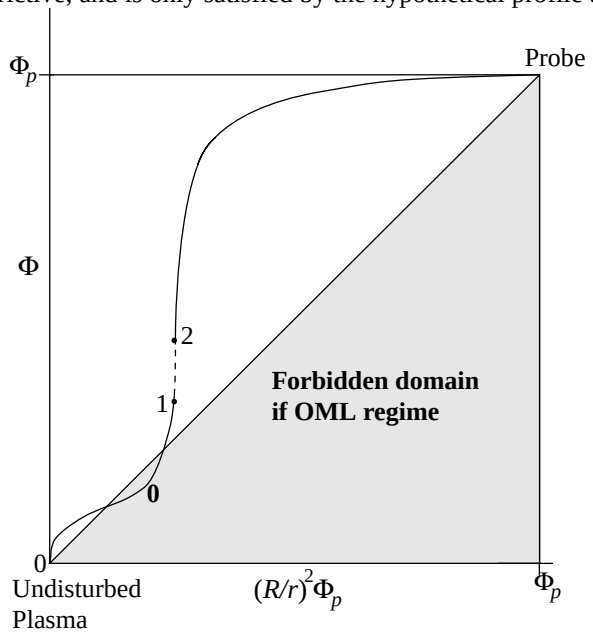

Figure 3. Potential profile for $R > R_{max}$. The plasma is quasi-neutral below point 1; below point 0 there are no potential barriers. The broad, ion-free region above the thin layers at points 1 and 2 is free of space-charge effects near the probe.

Figure 3 again shows the profile *d* of Fig.2 for the $R > R_{max}$ case. In order to solve Poisson's equation using (7), we need $J_r^*(E)$ in the different regions of the profile, and the particular function $J_R^*(E)$, which gives the current I too. The no-barrier condition (12), $J_r^*(E) = J_r(E)$ for all energies, holds below point 0. Property (11) may be illustrated by considering the r-family of straight lines $J^2 = J_r^2(E)$ in the E-J^2 plane, for the range $r \ge r_0$ (Fig.4a): for r increasing, the corresponding line keeps moving to the right for all positive energies. Since point 0 lies below the diagonal in Fig. 3, its line reaches to the left of the R-line on the J^2 axis.

The quasineutrality approximation for Eq.(2), $N_e \approx N_i$, is valid below a point 1 where $d\Phi/dr \to -\infty$ (Fig.3). Between points 0 and 1, there is an r-dependent energy range with potential barrier. Since we have $r_1 < r_0$ and $r_1^2\Phi_1 > r_0^2\Phi_0$, the r-lines for points 0 and 1 meet at some positive energy, as shown in Fig.4b. Also shown is the envelope $J^2 = J_{env}^2(E)$ of the set of r-lines in the range $r_1 < r < r_0$, which is determined by the equations $J^2 - J_r^2(E) = 0$, $\partial [J^2 - J_r^2(E)] / \partial r = 0$, leading to the parametric representation

$$J^2 = J_{env}^2(r) \equiv -m_e r^3 e \, d\Phi/dr, \qquad (13a)$$

$$E = E_{env}(r) \equiv -e\Phi(r) - 1/2 \, re \, d\Phi/dr \; . \qquad (13b)$$

The envelope touches each r-line at the E, J^2 point given by Eqs.(13a, b). Since E and J^2 diverge with $-d\Phi/dr$ in (13a, b), as $r \to r_1$, the envelope is asymptotic to the r_1-line; also, it is tangent to the r_0-line at $E = 0$ (Fig.4b). Condition $E_{env}(r) = 0$ in (13b) corresponds to a minimum of $r^2\Phi$, the profile tangent meeting the origin in Fig. 3 when point 0 is reached from above. The quasineutral solution below 0 has no such property, thus breaking down at that point; local use of the full Eq. (2),

however, suffices to round the profile at 0, with no effect beyond its immediate neighborhood. Point 0 will just be the point closest to 1 in the quasineutral, no-potential-barrier, solution.

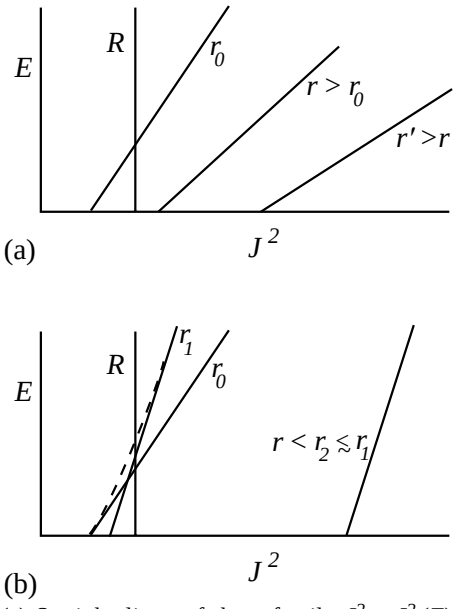

Figure 4. (a) Straight lines of the r-family $J^2 = J^2_r(E)$, defined in Eq.(5), for probe point 0 in Fig.3, and any two radii $r' > r$ beyond r_0. (b) Envelope $J^2_{env}(E)$ (dashed curve) for r-family lines in the range $r_1 < r < r_0$, and limit lines for points 0 and 1. At the top of the thin layers, and for most of the broad region above in Fig.3, r-lines lie far to the right; as the probe is approached, however, the r-line would move back to the left, finally reaching the probe line.

A simple but accurate approximation for $J_{env}(E)$ can now be readily obtained without knowledge of $\Phi(r)$, using the r_0 and r_1 lines in Fig.4b,

$$J_{env}^{\ 2}(E) = J_{r_1}^{\ 2}(E) - \frac{2m_e(r_1^{\ 2}e\Phi_1 - r_0^{\ 2}e\Phi_0)^2}{r_1^{\ 2}e\Phi_1 - r_0^{\ 2}e\Phi_0 + (r_0^{\ 2} - r_1^{\ 2})E}, \qquad (14)$$

where the values r_0, Φ_0, r_1, and Φ_1 are yet unknown. For any radius r between r_1 and r_0 we would now have

$$J_r^*(E) = J_{env}(E) \quad \text{for } E < E_{env}(r), \qquad (15a)$$

$$= J_r(E) \text{ for } E > E_{env}(r)\ . \qquad (15b)$$

As r approaches r_1, one has $E_{env}(r) \to \infty$ in (13b), Eq.(15a) for $J_r^*(E)$ then holding throughout the entire range $0 < E < \infty$. Above point 1 in Fig. 3 the potential Φ rises rapidly to values $\Phi >> \Phi_1$. Note that both $e\Phi_0$ and $e\Phi_1$ are of order of kT_i, whereas $e\Phi_p/kT_i$ is very large (~ 10^3, 10^4 for tethers); if Fig. 3 were drawn to scale, the near-vertical potential rise up from point 1 would occur very close to the Φ -axis, and point 0 would lie very close to the origin. With the r-line moving far to the right in Fig.4b as Φ rises, we still have $J_r^*(E) = J_{env}(E)$.

Finally, as one approaches the probe, moving toward the upper right corner in the diagonal of Fig. 3, the r-line moves back to the left in Fig.4b, ending at the R-line. As it follows from Fig. 4b and the preceding discussion, we have $J_R^*(E) = J_{env}(E)$ below the energy where the envelope crosses to the right of the near-vertical R-line. We now assume that R/R_{max} is large enough, with the crossing occuring at large E/kT_e. One may then safely set $J_R^*(E) = J_{env}(E)$ for all energies in the integrals of Eqs. (7) and (8). We also have $J_r^*(E) = J_{env}(E)$ from point 1 to the probe.

The ratio I/I_{OML} takes now the form

$$\frac{I}{I_{OML}} = \int_0^\infty \frac{dE}{kT_e} \exp\left(\frac{-E}{kT_e}\right) \frac{J_{env}(E)}{J_R(0)}\ . \qquad (16)$$

To obtain the values r_0, Φ_0, r_1, and Φ_1 that determine $J_{env}(E)$ in (14), we solve Poisson's equation with $J_R^*(E) = J_{env}(E)$ in (7) throughout. The quasineutrality relation at point 0, with $J_r^*(E) = J_r(E)$ in Eq.(7), and both the quasineutrality relation with $J_r^*(E) = J_{env}(E)$, and its derivative with respect to Φ at r_1, where $dr/d\Phi$ vanishes, serve to determine $e\Phi_0/kT_e$, $e\Phi_1/kT_e$, and r_1/r_0 as functions of T_i/T_e. Above point 1 there are two non-quasineutral layers that take the solution to values satisfying $\Phi_1 << \Phi << \Phi_p$, and to a radius r_2 a bit closer to the probe; the structure of these two thin layers can be analysed in a simple way, and yields r_2/r_1 and the behavior $\Phi \propto (r_1 - r_2)^{4/3}$ at the top of the second layer.[2]

In the broad region from these layers to the probe, we have $e\Phi/kT_i \sim \Phi/\Phi_1$ large (Fig.3), making N_i/N_∞ exponentially small in Poisson's equation; also, since r- lines lie far to the right in Fig.4b, we have $J_r^*(E) = J_{env}(E) << J_r(E) \approx J_r(0)$, considerably simplifying the integral for N_e/N_∞ in (7):

$$\frac{N_i}{N_\infty} \approx 0, \quad \frac{N_e}{N_\infty} \approx \frac{I}{I_{OML}} \frac{R}{\pi r} \sqrt{\frac{\Phi_p}{\Phi}}\ ; \qquad (17a, b)$$

although this approximation fails within some neighborhood of the probe, the high bias makes space-charge effects negligible there (even though R is not small compared with λ_{De}, λ_{Di}).[2] Using (17a, b), and matching to the second layer at $r_1 \times r_2/r_1$, one fully determines the solution $\Phi(r)$ to Poisson's equation in this broad region. The boundary condition $\Phi = \Phi_P$ at $r = R$, yields a fourth relation and serves to determine r_1.

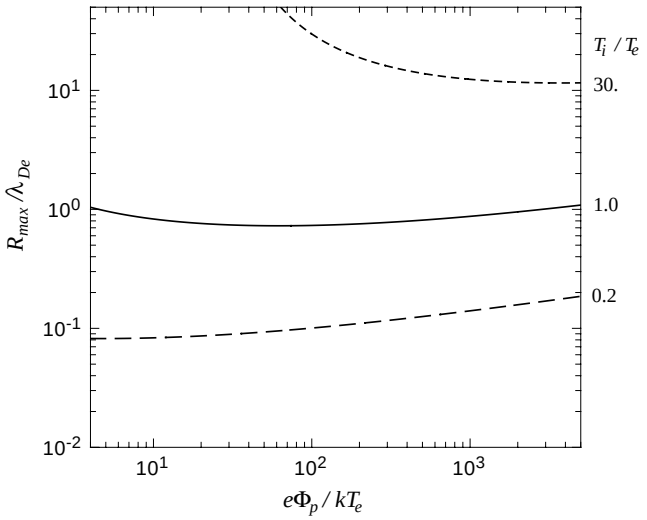

Figure 5. R_{max}/λ_{De} versus $e\Phi_P/kT_e$ for three values of temperature ratio T_i/T_e.

Figure 5, taken from results in Ref. 2, shows R_{max}/λ_{De} versus $e\Phi_P/kT_e$ and T_i/T_e; at any given bias, R_{max} increases with the T_i/T_e ratio. Figure 6 shows results from our present calculations for I/I_{OML}. Each curve reaches the value $I/I_{OML} = 1$ at a radius $\tilde{R}_{\max}$ larger than R_{max} (See Fig. 5). This is a conse-

quence of our having used the approximation $J_R^*(E) = J_{env}(E)$, which is only valid for R/R_{max} large enough; results valid for the entire range $R/R_{max} > 1$ are the subject of a future publication. The present, simplified results, giving $I/I_{OML} = 1$ for $R_{max} < R < \tilde{R}_{\max}$ and I/I_{OML} dropping rapidly beyond $\tilde{R}_{\max}$, are qualitatively correct, however, and lead to some simple conclusions:

1) One might use tethers with R larger than R_{max}, but not larger than $\tilde{R}_{\max}$.

2) The ratio $\tilde{R}_{\max}/R_{max}$ increases rapidly with decreasing T_i/T_e.

3) $\tilde{R}_{\max}$, in opposition to R_{max}, exceeds λ_{De} for quite small values of T_i/T_e.

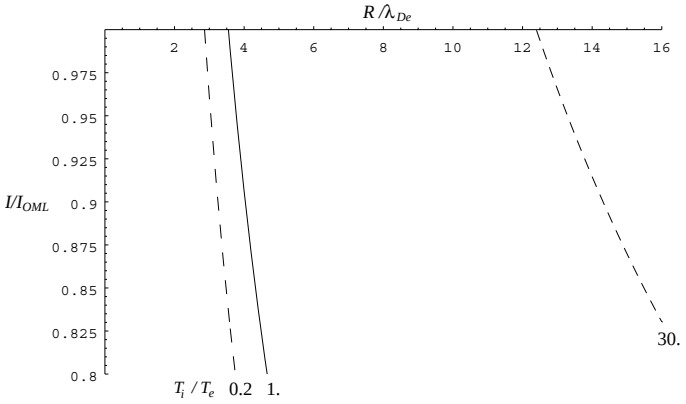

(a) $e\Phi_p/kT_e = 3000$.

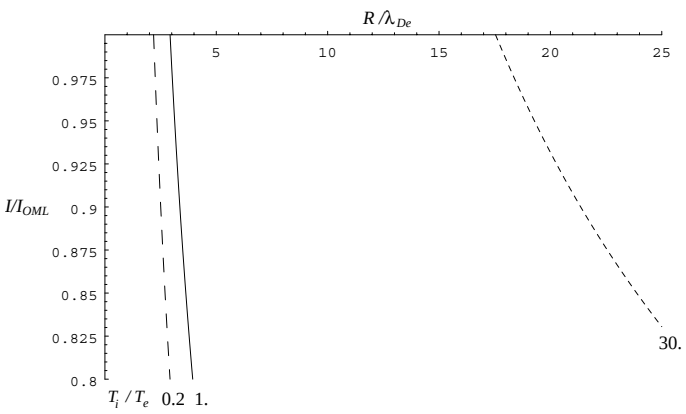

(b) $e\Phi_p/kT_e = 300$.

Figure 6. Normalized current I/I_{OML} versus R/λ_{De}, for $e\Phi_P/kT_e$ = 3000 (a) and 300 (b), and three values of T_i/T_e. In our approximate solution (strictly valid for R/R_{max} large), the ratio I/I_{OML} remains equal to unity between R_{max} and some value $\tilde{R}_{\max}$.

These conclusions are relevant to the design of bare tethers, which find a plasma with Debye length and, to some degree, ratio T_i/T_e varying along the orbit; this is more so if the tether is used for orbit raising or lowering. The conclusions also support a point made in Ref.1, concerning the effect of a plasma velocity U relative to the probe. This introduces a new characteristic (ram) ion energy, which, for a tether orbiting in the F layer, is large compared with the thermal energy,

$$1/2\ m_i U^2 \approx 4.5\ \text{eV} >> kT_i \sim 0.15\ \text{eV}$$

(at higher altitudes, with H or He ions—and weakly reduced U^2—, the two energies are comparable). The unperturbed ion distribution function is now strongly nonisotropic, and the electric field is non radial.

Note that the OML current law is still valid, being independent of both ion distribution function and cross-section shape (just replace $2R$ with $perimeter/\pi$ in Eq.1); the law applies even if the potential has no rotational symmetry.[2] The high-bias limit law (1) is particularly robust: it is also independent of the unperturbed electron distribution function as long as it is isotropic, as in the present case, with $1/2\ m_e U^2 << kT_e$. The effect of a large ion ram energy would just be a reduction of the domain of validity for the OML law.

The fact that I/I_{OML} remains unity over some domain in Fig.5 mirrors the fact that I_{OML}/I_{th} in (1) is independent of R/λ_{De}, and T_i/T_e. Figures 6a, b extend the case for I/I_{OML} close to unity to a much larger domain. This means that one could alter substantially, say T_e or T_i, or the probe cross section (keeping its perimeter), thus fully modifying the structure of the potential field, without reaching the boundary of the domain of OML validity, that is, with no current I variation. This is a case quite the opposite of large spherical collectors, as used in the TSS1 tethers. In predicting the new domain of validity (instead of an actual value for I) one might use crude models, if conservative.

For the conditions of interest, $1/2\ m_i U^2 << e\Phi_p$, ions would be kept far away from the probe for all directions, with some (angle dependent) potential structure similar to that shown in Fig.3. In a crude model, one would ignore the nonthermal character of the ram energy, excepting the fact that it makes the ion characteristic energy angle dependent; for all other parameters fixed, the distance r_0 in Fig.3 (and for *b-d* profiles in Fig.2) is directly related to the characteristic ion energy.[2] In a plasma with $T_i \sim T_e$, one would then have effective ion temperatures $kT_i(eff) \sim 1/2\ m_i U^2 \sim 30\ kT_e$ on the windward side, and $T_i(eff) \sim T_e$ on the lateral sides. For the lee side, we take $r_0(\text{lee}) \sim r_0(\text{side}) \times \sqrt{m_i U^2 / 2kT_e}$ from simple wake considerations, and $r_0 \sim R\sqrt{e\Phi_P / kT_i}\sqrt{T_e / T_i}$, for T_i/T_e small or about unity from the no-U analysis,[2] yielding $T_i(eff) \sim T_e \times \sqrt{2kT_e / m_i U^2} \sim 0.2\ T_e$. One can now see from Figs.5 and 6a, that a probe with $e\Phi_P \sim 3000\ kT_e$ and $R \le R_{max}$ ($T_i/T_e \sim 1$, $U = 0$) $\sim \lambda_{De}$, has R well below $\tilde{R}_{\max}$ for all three values $T_i/T_e \sim 0.2$, 1, and 30; this suggests the probe should collect current close to the OML value in Eq.(1).

The work of J.R.S. was supported by the Comisión Interministerial de Ciencia y Tecnología of Spain under Grant PB97-0574-C04-1.

References

1 J. R. Sanmartín and R. D. Estes, Validity of the Orbital-Motion-Limited regime of Cylindrical Probes, *Proc. Tether Technology Interchange Meeting*, ed. J. Harrison, NASA CP-206900, 399 (1998).

2 J. R. Sanmartín and R. D. Estes, *Phys. Plasmas* 6, Jan. (1999).

3 J. R. Sanmartín, M. Martínez-Sanchez, and E. Ahedo, *J. Propul. Power* 9, 353 (1993).

4 R. D. Estes, J. R. Sanmartín, and M. Martinez-Sanchez, Technology of Bare Tether Current Collection, submitted to *J. Spacecraft Rockets* (1998).

5 L. W. Parker, Computer Method for Satellite Plasma Sheath in Steady-State Spherical Symmetry, Air Force Cambridge Research Laboratories, Report No. AFCRL-TR-75-0410 (1975).